Surface & Coatings Technology 205 (2011) 5464–5469

Contents lists available at ScienceDirect

Surface & Coatings Technology

journal homepage: www.elsevier.com/locate/surfcoat

Development and thermal evolution of silver clusters in hybrid organic–inorganic sol–gel coatings

R. Procaccini, S. Ceré, S. Pellice *

Instituto de Investigaciones en Ciencia y Tecnología de Materiales (INTEMA), UNMdP-CONICET, Av. Juan B. Justo 4302. B7608FDQ Mar del Plata, Argentina

ARTICLE INFO

Article history:
Received 17 December 2010
Accepted in revised form 9 June 2011
Available online 17 June 2011

Keywords:
Silver clusters
Sol–gel
Biocide coatings
SAXS fitting
Silver release

ABSTRACT

A silver doped hybrid organic–inorganic sol–gel coating was developed through the hydrolytic condensation of tetraethoxysilane (TEOS) and methyl-triethoxysilane (MTES). Silica nanoparticles were added in order to give a mechanical reinforcement and silver nitrate as the supplier of Ag^+ ions, which have a potential effect as a biocide component. Synthesis of precursor sol and the evolution of silver clusters in the whole process were analyzed through Attenuated Total Reflectance Fourier Transformed Infrared spectroscopy (ATR-FTIR) and UV–visible spectroscopy. A high thermal sensitivity of sub-nanometric silver particles was determined by Small Angle X-ray Scattering (SAXS) carrying to formation of higher agglomerates or silver nanoparticles. Lixiviation tests show long-term and gradual silver releasing without worsening of the structural integrity of coatings.

1. Introduction

The development of new materials enriched with noble metal ions, such as silver, cobalt or copper, is of great interest in the field of hygienic and healthiness products due to its action against fungus and bacteria. Although a large number of commercial products are chemically active against microorganisms, they are usually limited to fabrics for medical bandages and sportswear in order to avoid, respectively, infections and odors. Although many of those products are based on the biocide properties of silver nanoparticles, it is well known that Ag^+ ions have an effective action against bacteria life inhibiting their DNA replication process, increasing the permeability of the cytoplasmic membrane and inhibiting the respiratory enzymes, causing asphyxia of the bacteria. Taking this feature in account, reduction of silver ions must be avoided in order to maximize the biocide character of the functional coating.

Natural trend of silver to reduce and form metallic particles makes its incorporation as ions or small clusters quite difficult in hybrid organic–inorganic solid matrixes. This property is usually leveraged to synthesize suspensions of spherical nanoparticles, through emulsion routes [1–5], or solid materials loaded with "in situ" generated nanoparticles [6–9].

In this work, the development of silver doped hybrid organic–inorganic sol–gel coatings is focused. A hybrid organic–inorganic matrix was obtained through the hydrolytic condensation of tetraethoxysilane (TEOS) and methyl-triethoxysilane (MTES). Silver nitrate ($AgNO_3$) was added as supplier of Ag^+ and silica nanoparticles were added to increase the coating density and to improve the mechanical properties.

A characterization was performed in sols and in the resulting dip-coated films in order to determine the evolution of silver ions and clusters along the whole process. Small Angle X-ray Spectroscopy (SAXS) was performed with synchrotron light, which is a powerful tool for characterization of size distribution of particles, even sub-nanometric and small clusters [3,7–13]. Silver lixiviation process was studied on immersed samples through X-ray Fluorescence Spectroscopy (XRF).

2. Experimental

Hybrid sols were prepared by the chemical reaction of tetraethoxysilane (TEOS) and methyl-triethoxysilane (MTES) in presence of an aqueous dispersion, 40 vol.%, of colloidal silica (SiO_2 NP, LUDOX AS-40 Aldrich, mean size: 6 nm). TEOS/MTES/SiO_2 (NP) molar ratio was kept at 36/54/10. Besides of the water supplied by Ludox, an additional aliquot was added in order to reach a molar ratio ethoxy groups/water of 2. Hydrolytic condensation was acid catalyzed at room temperature by the addition of concentrated HNO_3 in a 0.6 vol.%. Because alkoxydes and water are immiscible phases, an emulsion-like structure was formed under vigorous stirring, at 1500 rpm, prior to catalysis; then, the chemical reactions spontaneously take place carrying to a homogeneous sol.

Silver doping was performed through the addition of a pyridine stabilized solution of $AgNO_3$ and absolute ethanol. Pyridine/Ag molar ratios of 2/1 and 1/1 were analyzed in this work. By mixing the appropriated amounts of hybrid sol and silver solutions, the precursor sols for silver doped sol–gel coatings were obtained, with 1, 2 and 3 mol % of Ag with respect to the silica of the hybrid matrix of resulting coatings.

* Corresponding author. Tel.: +54 223 4816600; fax: +54 223 4810046.
E-mail address: spellice@fi.mdp.edu.ar (S. Pellice).

0257-8972/$ – see front matter © 2011 Elsevier B.V. All rights reserved.
doi:10.1016/j.surfcoat.2011.06.018

Evolution of hydrolytic condensation and formation of coordination compounds of silver were analyzed by Fourier Transformed Infrared Spectroscopy (Nicolet 6700 FTIR Spectrometer, Thermo Electron Corporation) by Attenuated Total Reflectance (ATR).

Through the dip-coating process, at 25 cm/min of withdrawal speed, homogeneous coatings were deposited on microscope glass slides. After drying, coatings were exposed to thermal treatments of either 30, 150, 300 or 450 °C, in air atmosphere during 30 min resulting in slightly translucent and yellowish coatings.

Chemical stability of silver in precursor sols was analyzed through UV–visible spectroscopy (UV-160A, Shimadzu) in transmission mode. Non-diluted sols were analyzed through a 10 mm quartz cell along storing at 4 °C and protected from light. A non-doped sol was used as reference sample. UV absorption of coatings was also analyzed in transmission mode.

Development of silver nanoparticles in coatings, as a function of pyridine/silver ratio and thermal treatment, was analyzed through Small Angle X-ray Scattering (SAXS) using the beam lines SAXS1 and SAXS2 of the National Laboratory of Synchrotron Light (LNLS, Campinas, Brazil). Although thin films are usually probed under a grazing incidence of the X ray beam (GISAXS) in order to determine a spatial distribution with preferential orientation or gradients in the concentration of nanoparticles [14–16], in preliminary studies performed by GISAXS to this kind of sol–gel coating, as reveled by isotropic 2D images, neither preferential orientation nor ordering of silver particles were observed. Thus, a simpler setup in transmission mode of the X ray beam is very useful to analyze the size distribution of nanoparticles developed in our case. Coatings were taken out from glass substrates by scratching producing glassy powders which were placed in the sample holders by adhesive polyimide film (Kapton®, DuPont). In order to subtract the contribution of the adhesive tape from SAXS spectra, Kapton film was used as background. The collimated beam crossed the samples through an evacuated flight tube and was scattered to 2D CCD marCCD detectors with active areas of 28 cm^2 (SAXS1) and 16 cm^2 (SAXS2) with pixel sizes of, respectively, 172 μm and 316 μm. To cover a wide range in the q-space, two geometrical configurations were set up, a sample detector distance of 80 mm with monochromatic light of $\lambda = 1.608$ Å (SAXS1) and a sample detector distance of 614 mm with monochromatic light of $\lambda = 1.488$ Å (SAXS2). The Q range was calibrated using silver behenate, which have a well-known lamellar structure with $d = 5.848$ nm. The isotropic 2D scattering patterns were collected after exposure times of 500 s (SAXS1) and 20 s (SAXS2). The images were corrected by taking into account the detector dark noise and normalized by the sample transmission considering the 360 azimuthal scan. This procedure was carried out using the FIT2D software [17]. SAXS data were processed by the SASfit software package [18] using the theoretical values of the X-ray scattering length densities of silver (7.744×10^{-3} nm^{-2}), silica (1.922×10^{-3} nm^{-2}) and the hybrid matrix (1.140×10^{-3} nm^{-2}) for the fitting procedure. SAXS results were fitted according to a bimodal Schultz–Zimm distribution (SZ) of spherical solid silver and silica nanoparticles. The Schultz–Zimm distribution (Eq. 1), derived from thermodynamical theories, is of particular importance and has a better match to reality than the normal Gaussian distribution to describe particles distribution [19].

$$SZ(R,N,R_a,k) = \frac{N}{R_a}\left(\frac{R}{R_a}\right)^{k-1}\frac{k^k\ \exp(-kR/R_a)}{\Gamma(k)} \quad (1)$$

where the parameter k of the size distribution is related to the variance σ by $k = 1/\sigma^2$. R_a is the scaling parameter and defines the maximum of the size distribution for large values of k. $SZ(R,N,R_a,k)$ is normalized so that (Eq. 2):

$$\int_0^\infty SZ(R,N,R_a,k)dR = N. \quad (2)$$

Lixiviation process of silver was recorded along 48 days of immersion in deionized water at 30 °C keeping an immersed surface/water ratio of 0.4 cm^2/ml. X-ray Fluorescence Spectroscopy (XRF, MiniPal 2, PANalytical) was performed at 5 kv and 650 μA in He atmosphere. Silver release was determined as a function of the band area corresponding to the electronic transition Lα of Ag atoms at 2.982 keV. XRF curves fittings were performed by Origin software (OriginPro 8 SR0, v8.0724 (B724), OriginLab Corporation) giving R^2 values between 0.9988 and 0.9993, corresponding to numerical errors between 4.57 and 6.25%.

Coated samples, before and after silver lixiviation, were observed by Scanning Electron Microscopy (SEM, Jeol 6460). A very thin gold–palladium film was sputtered onto samples in order to improve their surface electric conductivity.

3. Results and discussion

3.1. Synthesis and characterization of sols

FTIR analysis allows the observation of the whole process trough the following of bands corresponding to the chemical groups involved. Table 1 displays the main FTIR bands appearing. Hydrolytic condensation of TEOS and MTES in presence of the aqueous suspension of silica nanoparticles occurs fast and spontaneously after addition of HNO_3 to catalyze the chemical reaction. Fig. 1 shows FTIR spectra of main reagents and its resulting sol. Suspension of silica nanoparticles presents a sharp band centered at 1104 cm^{-1} and a less intense and broad shoulder around 1200 cm^{-1} corresponding, respectively, to the transversal optic (TO) and the longitudinal optic (LO) modes of the asymmetrical vibration of silica. Also in the SiO_2 (NP) suspension, a wide band at 1638 cm^{-1}, attributed to water, is observed. After the hydrolytic condensation, bands related to the reactive ethoxy groups from both TEOS and MTES, at 1169, 1075 and 961 cm^{-1}, and the corresponding one of water, undergo a strong diminution. At the same time, as a consequence of hydrolysis and condensation, ethanol bands develop and are clearly observed at 1080, 1045 and 880 cm^{-1}. Bands

Table 1
FTIR bands of reagents and products of the hydrolytic condensation. [20–30].

Component	Wavenumber (cm^{-1})	Assignment
TEOS	1169	δ(CH_3)
	1102	ν_{as}(C—C + C—O) and δ(COH)
	1075	ν_{as}(Si—O—C)
	961	δ(H_3CO) and δ(H_3CC)
	787	ν(Si—O + C—O)
MTES	1275	δ($SiCH_3$)
	1161	δ(CH_3)
	1075	ν_{as}(Si—O—C)
	961	δ(H_3CO) and δ(H_3CC)
	810	ν_{as}(Si—O—C)
	778	ν(Si—O + C—O)
H_2O	1638	δ(OH)
Ethanol	1088	ν_{as}(C—C + C—O) and δ(COH)
	1045	δ(CCH_3) and δ(COH)
	880	ν_s(C—C + C—O)
Si—O—Si	1150, 1200	ν_{as} LO
	1113–1120	ν_{as} TO
	1045, 1080 and 1100	ν_{as} TO
Non-bridging oxigens	975	ν(Si—OH)
	940–960	ν(Si—OH)
	915	ν(Si—O^-)
	790–810	δ_s(Si—O)
Pyridine	1591	ν(C—C)
	1442	ν(C—C)
	1215	β(C—H)
	1001	δ(N—C)
	750	γ(N—C)
	706	γ(C—H)

ν—stretching; δ—bending; β—in-plane deformation; γ—out-of-plane deformation.

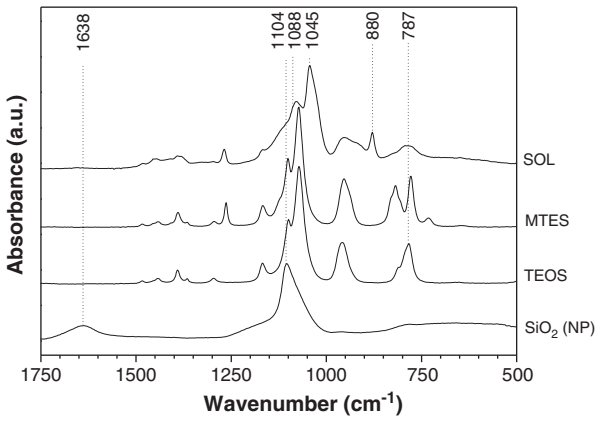

Fig. 1. FTIR spectra of main reagents and of the resulting sol after the hydrolytic condensation.

corresponding to the transversal optical (TO) mode of the asymmetrical vibrations of the Si—O—Si bonds, at 1080 and 1045 cm^{-1}, characteristic of a less dense sol–gel hybrid organic–inorganic silica network, are overlapped to the sharper ethanol bands.

Dilution of $AgNO_3$ in a pyridine/ethanol solution carries to the formation of a coordination compound allowing the stabilization of Ag^+ ions in solution. Fig. 2 shows the shift in the absorption bands of pyridine as a consequence of the ionic-molecular perturbation characteristic of its coordination with silver atoms. Vibrations of uncoordinated pyridine, at 1591, 1442, 1215, 1001, 750 and 706 cm^{-1}, shift, respectively, to 1602, 1448, 1220, 1012 (sh), 755 and 702 cm^{-1}. Pyridine molecules that have not been incorporated into the first coordination sphere of the Ag^+ ion should posses the same spectrum in solution as the molecules of the pure solvent. [20] So, as the ionic-molecular perturbation extends only to the directly coordinated molecules, all of them are coordinated to Ag^+ ions.

After mixing of the previously hydrolyzed sol and the silver/pyridine solution, no change was observed in its colorless and transparency remaining as a long term stable sol, up to 3 months of storing at 4 °C and keeping from light. FTIR spectra of resulting sol (not showed) suggest no changes in coordination state of silver/pyridine compounds along storing time.

Pyridine based stabilization of silver doped sols, carried out to a suspension of silver clusters. UV–visible spectra of silver doped sols, Fig. 3a, show two intense bands with maximums at 272 and 305 nm attributed, respectively, to Ag_4^{2+} and Ag_2^+ clusters. [31] Besides of pyridine coordination, proportionally to silver content, a fraction of Ag^+ ions reduce quickly to Ag_2^+ clusters in presence of residual water and the

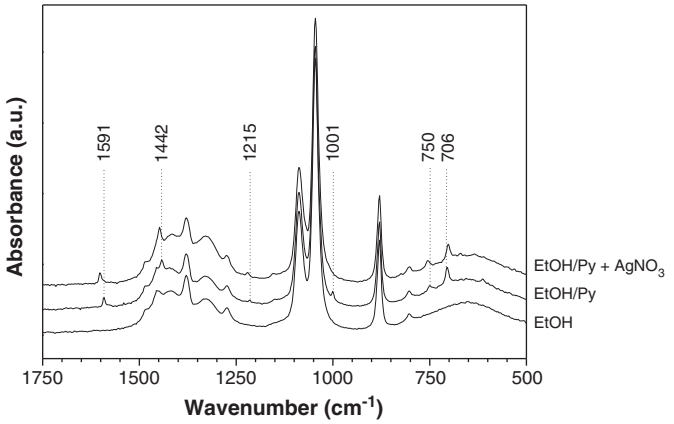

Fig. 2. FTIR spectra of pyridine stabilized silver solution.

organic components of the hybrid sol. Zhang et al. [32] observed that formation of small silver clusters occurs extremely fast in aqueous solutions. As silver content increases to 2 and 3 mol%, a new band at 285 nm develops probably due to formation of Ag_8 or higher clusters [33,34]. Even with pyridine coordination, upon aging, silver doped sols showed high stability with a negligible trend to form agglomerates and silver colloids or nanoparticles. Fig. 3b shows the UV–visible spectra of a 1% Ag doped sol along storing at 4 °C and protected from light. A very weak and wide shoulder around 400 nm, attributed to the plasmonic band of spherical silver nanoparticles [32,35,36], is developed. This phenomenon is consequently associated with a slight diminution of the bands of silver clusters.

3.2. Thermal evolution of Ag doped coatings

After dip-coating, drying and thermal treatment, the matrixes of obtained films acquire hardness and get a denser structure. On the other hand, silver ions and clusters are susceptible to undergo a process of loosening of pyridine coordination and the consequent destabilization of the arrangement achieved by silver in the sol state, this phenomenon gives place to coalescence and agglomeration processes producing higher silver nanoparticles. [37]

Through SAXS experiments, performed with synchrotron radiation, a detailed analysis of particle distribution could be done. Fig. 4a shows, as instance, the SAXS spectrum and fitting of a sample obtained from a 3% Ag sol, with Py/Ag ratio of 2, thermally treated at 30 °C. In this case, the experimental setup allows a good determination of the baseline

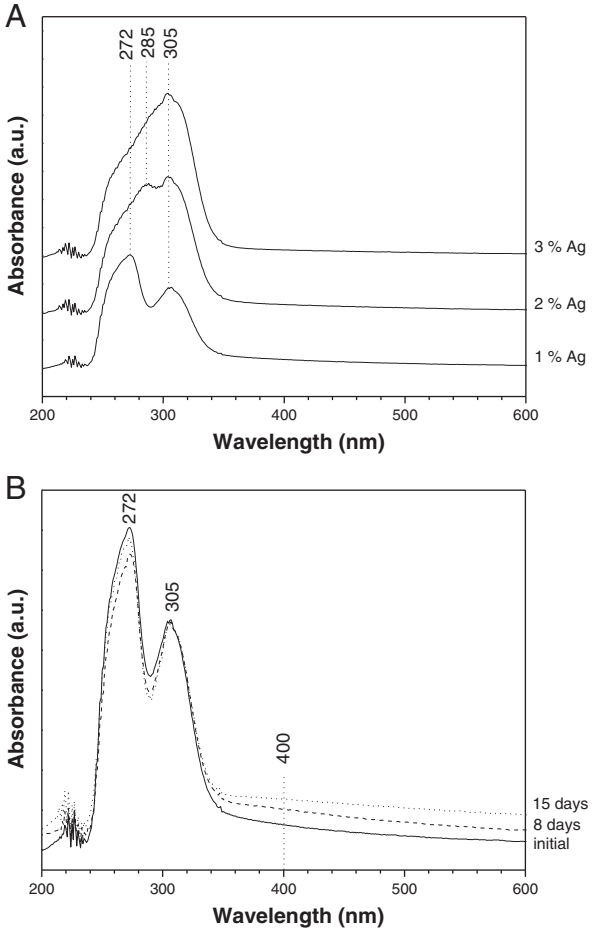

Fig. 3. UV–visible spectra of a) silver doped sols as a function of silver molar content and b) of aging of 1 mol% Ag doped hybrid sol along storing at 4 °C.

from the asymptote at higher q values. Three main components are clearly observed: a) a curve characteristic of a sol–gel matrix [12], b) a wavy line, attributed to a narrow size distribution of silica nanoparticles and c) a curve corresponding to silver clusters. Due to the double logarithmic scale, it is noticeable that silver clusters have the higher contribution at $q > 1\ nm^{-1}$ values. Fig. 4b shows SAXS curves, and their corresponding fits, of samples doped with 3 mol% Ag, Py/Ag ratios of 1 and 2, and thermally treated at 30 and 150 °C.

The process of hydrolytic condensation in presence of silica nanoparticles produces their surface modification (grafting) through covalent bonding to partially hydrolyzed TEOS and MTES. As hydrolysis and condensation progress, nanoparticles superficially enriched with Si—OH groups, undergo agglomeration growing from 3 nm to 14.5 nm of radius approximately. This result is in according with a previous work were those silica nanoparticles were incorporated to a hybrid silica–methacrylate sol. [38] Although this silica agglomeration implies a hierarchical structure were agglomerates are composed by smaller silica nanoparticles, those constitutive nanoparticles are not revealed by SAXS experiments. Presumably, this effect is a consequence of a tight percolation of those silica nanoparticles during the hydrolytic process. Thus, silica nanoparticles would be embedded into a local matrix of similar light scattering density, which constitutes the observed agglomerates. Taking in account that this agglomeration occurs during the synthesis process, and that those agglomerates are covalently bonded to the hybrid matrix by Si—O—Si bonds, it is clear that no changes are possible in their size distribution as a function of the thermal treatment of coatings, as it was experimentally observed. Fig. 5 displays the particle size distribution of silica nanoparticles, from the fitting procedure of SAXS curves, present in 3% Ag doped coatings thermally treated at 30

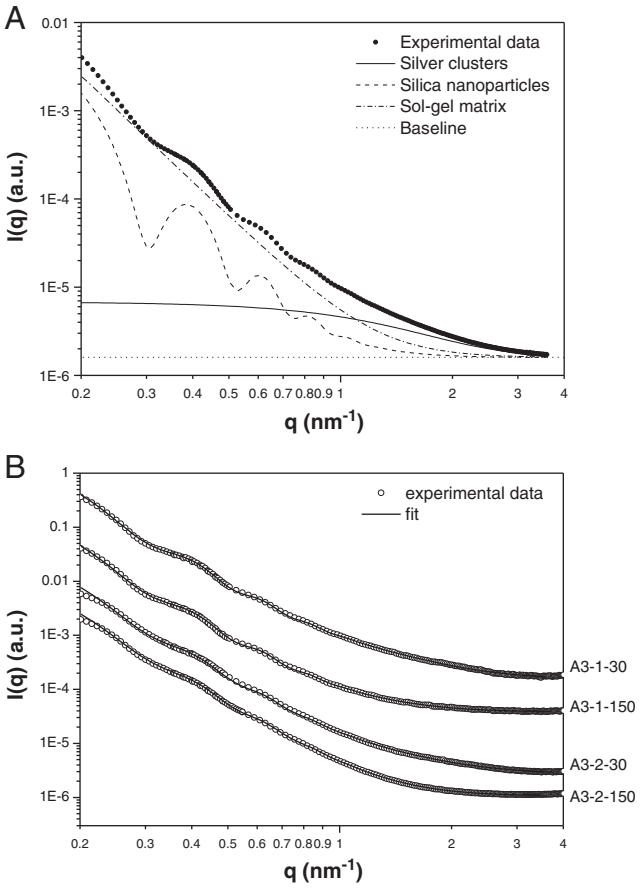

Fig. 4. SAXS spectra of 3 mol% Ag doped coatings. a) Components of the fitting for a sample thermally treated at 30 °C with a molar ratio Py/Ag = 2 and b) experimental data and corresponding fitting curves.

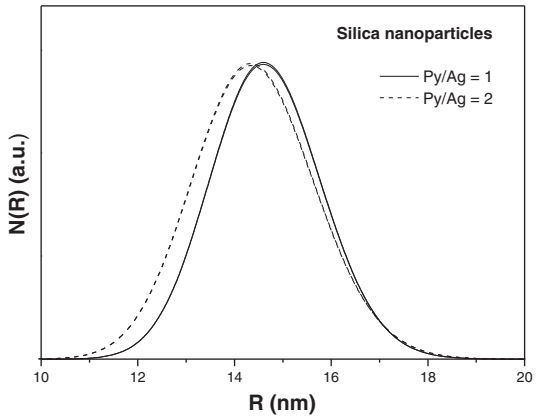

Fig. 5. Size distribution of silica nanoparticles on samples with 3 mol% of Ag thermally treated at 30 and 150 °C.

and 150 °C with different Py/Ag ratios. As it is observed, temperature has no effect on silica nanoparticles size distributions, curves corresponding to 30 °C and 150 °C are perfectly superimposed; only a small difference, attributed to the normal differences of sols synthesized in separate batches, is revealed with the Py/Ag ratio.

During deposition, drying and thermal treatment of silver doped coatings, a strong change occurs to silver clusters. SAXS fittings reveal the evolution of subnanometrical silver particles in a monomodal size distribution with the mode around of 0.3 nm of radius, Fig. 6. Such particle size agrees with the matching for Ag_8 clusters and its isomeric ions (ca. 5 Å diameter) [34]. Those clusters were also seen by UV–visible spectroscopy through its band at 285 nm (Fig. 3). Smaller clusters are not detectable by SAXS experiments under the used instrumental settings. Two well differenced behaviors were observed as Py/Ag ratio increases from 1 to 2. Although, at 30 °C, coatings with a ratio Py/Ag = 2 has approximately the twice of particles than coatings with ratio Py/Ag = 1, its distribution is slightly sharper and, as a result, the volumetric integration reveals that the amount of silver distributed in those clusters differs only by a 9.5%. Upon thermal treatment in air atmosphere, coordination between silver and pyridine is broken and the reduction of Ag^+ to Ag^0 takes place with agglomeration and growing of silver clusters and nanoparticles. Such reduction process is increased by interaction with the surrounding matrix and the organic components. Therefore, when coatings are exposed to a thermal treatment of 150 °C, an expectable diminution in the amount of silver clusters is observed; coatings with ratios Py/Ag = 1 and 2 loses respectively 54 and 92 vol.%. That loosening of silver clusters with temperature could impose strong limitations for production of biocide coatings with these processing

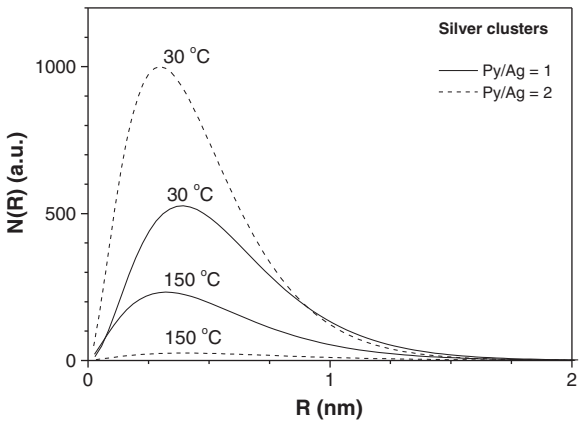

Fig. 6. Size distribution of silver clusters on samples with 3 mol% of Ag thermally treated at 30 and 150 °C.

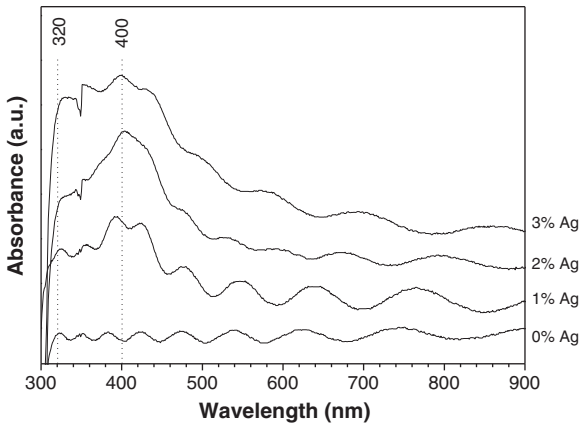

Fig. 7. UV–visible spectra of silver doped coatings as a function of silver content.

conditions. Falletta et al. [13] found bactericidal behavior in fabrics soaked with *ultra-small* silver particles (0.6 nm of radius) doped sols.

UV–visible spectra of silver doped coatings thermally treated at 450 °C, Fig. 7, reveal, enveloping the true UV–visible absorption signal, the characteristic fringe pattern of transparent films. Such pattern is the result of interference phenomenon present in thin films and is function of their thickness and refractive index. In spite of this, a plasmon band, corresponding to silver nanoparticles, around the 400 nm, and a shoulder, at lower wavelengths, can be observed. Considering that the signal at wavelengths lower than 300 nm is wholly absorbed by the silica of the substrate, the presence of a shoulder around 320 nm can be attributed to residual Ag_8 or other very small silver particles and clusters [34,36,39] retained in the hybrid structure after the thermal treatment.

3.3. Silver release

In order to possess effectiveness against microorganisms, silver ions should be capable to migrate from the hybrid matrix of the coatings. Fig. 8 shows the results of lixiviation tests performed on water at 30 °C of coatings containing 3% Ag. Although the experimental setting of lixiviation test is not representative of a particular use condition, two relevant observations can be done: a) silver is capable to migrate from the hybrid matrix and b) after a relatively fast releasing in the firsts days of test, a gradual silver liberation is achieved. This result clearly evidences the potential that this kind of coating has as long-term biocide treatments for hygienic surfaces.

Study of SEM micrographs of those coatings reveals a regular and dense film. Fig. 9a shows the transversal section of a fracture surface where the glassy film, of about 1.4 μm of thickness, is tightly adhered

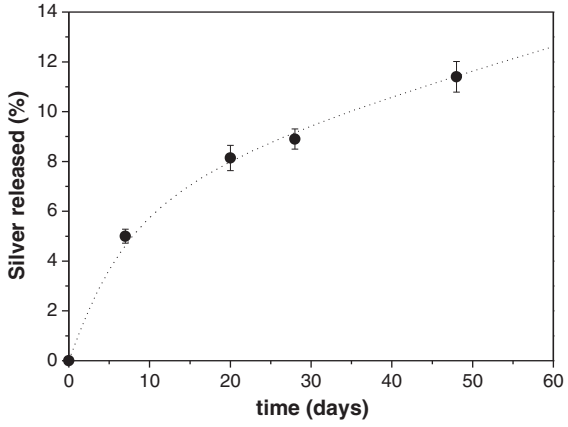

Fig. 8. Silver release from 3 mol% doped hybrid coating thermally treated at 450 °C.

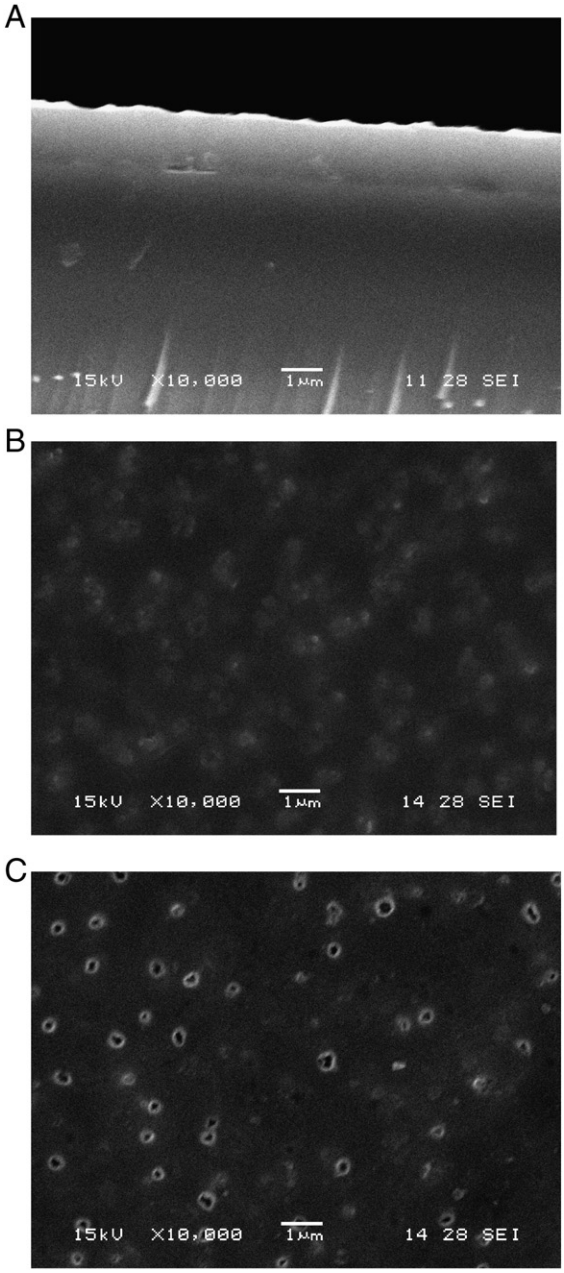

Fig. 9. Scanning electron micrographs of 3 mol% Ag doped coatings thermally treated at 450 °C. a) Transversal section, b) coating surface before lixiviation process and c) external surface after silver release.

on the substrate. Fig. 9b shows the external surface of the film in which the presence of regions with higher electronic contrast can be observed under its surface. Those regions can be certainly attributed to agglomerates of silver clusters and nanoparticles, as SAXS and UV–visible spectra revealed. After lixiviation tests, Fig. 9c, the partial silver release produces the clearing out of some of those Ag-rich regions leading to the formation of an analogous pattern of hollows and remnant Ag-rich regions. Besides of the damage produced by lixiviation on its surface, the hybrid coating still conserves its structural integrity without takeoff.

4. Conclusions

Silver doped hybrid organic–inorganic sol–gel coatings were synthesized by hydrolytic condensation of TEOS and MTES in presence of silica nanoparticles. Pyridine coordination of silver ions carried to the

development of Ag_2^+ and Ag_4^{2+} clusters and allowed the stabilization of sols for more than two months of aging in dark conditions at 4 °C without precipitation or loosening of colorless. Upon thermal treatment, silver clusters undergo agglomeration leading to formation of nanometric and sub-nanometric particles detectable by SAXS and UV–visible tests. Although sub-nanometric silver particles vanish almost totally at temperatures higher than 150 °C, a gradual silver release was observed in lixiviation tests indicating its ability to migrate through the hybrid organic–inorganic matrix. This fact validates the potential attitude of this kind of silver doped coatings to be active against microorganisms at long-terms.

Acknowledgments

Authors want to acknowledge the National Synchrotron Light Laboratory, Campinas, Brazil (LNLS, Project 6780/2010, proposal D11A-SAXS1-10004) and the Argentine National Agency for Scientific and Technological Promotion (ANPCyT PICT-2007-01161) for the financial support. Also the Argentine National Council of Scientific and Technical Researches (CONICET) is gratefully acknowledged.

References

[1] M. Arada, K. Kuramitsu, Y. Kimura, K. Saijo, Eng. Aspects 327 (2008) 21.
[2] M. Arada, C. Kawasaki, K. Saijo, M. Demizu, Y. Kimura, J. Colloid Interface Sci. 343 (2010) 537.
[3] M. Andersson, J.S. Pedersen, A.E.C. Palmqvist, Langmuir 21 (2005) 11387.
[4] A. Ledo, F. Martínez, M.A. López-Quintela, J. Rivas, Physica B 398 (2007) 273.
[5] C. Petit, P. Lixon, M.P. Pileni, J. Phys. Chem. 97 (1993) 12974.
[6] J. Compton, D. Thompson, D. Kranbuehl, S. Ohl, O. Gain, L. David, E. Espuche, Polymer 47 (2006) 5303.
[7] E.V. Shtykova, K.A. Dembo, V.V. Volkov, E.E. Said-Galiev, A.I. Stakhanov, A.R. Khokhlov, Nanotechnol. Russ. 4 (2009) 700.
[8] T. Saraidarov, V. Levchenko, R. Reinsfeld, Phys. Status Solidi C 7 (2010) 2648.
[9] V. Purcar, D. Donescu, C. Petcu, R. Luque, D.J. Macquarrie, Appl. Catal. A 363 (2009) 122.
[10] A.M. Signori, K.O. Santos, R. Eising, B.L. Albuquerque, F.C. Giacomelli, J.B. Domingos, Langmuir 26 (2010) 17772.
[11] A.F. Craievich, Mater. Res. 5 (2002) 1.
[12] J. Wang, J. Shen, B. Zhou, X. Wu, Nanostruct. Mater. 7 (1996) 699.
[13] E. Falletta, M. Bonini, E. Fratini, A. Lo Nostro, G. Pesavento, A. Becheri, P. Lo Nostro, P. Canton, P. Baglioni, J. Phys. Chem. C 112 (2008) 11758.
[14] M.M. Abul Kashem, J. Perlich, L. Schulz, S.V. Roth, P. Müller-Buschbaum, Macromolecules 41 (2008) 2186.
[15] M.M. Abul Kashem, J. Perlich, A. Diethert, W. Wang, M. Memesa, J.S. Gutmann, E. Majkova, I. Capek, S.V. Roth, W. Petry, P. Müller-Buschbaum, Macromolecules 42 (2009) 6202.
[16] S.V. Roth, M. Kuhlmann, H. Walter, A. Snigirev, I. Snigireva, B. Lengeler, C.G. Schroer, M. Burghammer, C. Riekel, P. Müller-Buschbaum, J. Phys. Condens. Matter 21 (2009) 264012.
[17] A.P. Hammersley, Scientific software FIT2D, European Synchrotron Research Facility, Grenoble, 2009 URL, http://www.esrf.eu/computing/scientific/FIT2D/.
[18] J. Kohlbrecher, Software Package SASfit for Fitting Small-Angle Scattering Curves, Paul Scherrer Institute, Villigen, 2010 URL, http://kur.web.psi.ch/sans1/SANSSoft/sasfit.html.
[19] T. Zemb, P. Lindner, Neutron, X-rays and Light: Scattering Methods Applied to Soft Condensed Matter, first ed. North-Holland Delta Series, Amsterdam, 2002.
[20] I.S. Perelygin, M.A. Klimchuk, J. Appl. Spectrosc. 24 (1976) 43.
[21] P.A. Joy, S. Vasudevan, J. Am. Chem. Soc. 114 (1992) 7792.
[22] M.L. Zheludkevich, M.G.S. Ferreira, I.M. Miranda Salvado, J. Mater. Chem. Rev. 15 (2005) 5099.
[23] J.H. Osborne, K.Y. Blohowiak, S.R. Taylor, C. Hunter, G. Bierwagon, B. Carlson, D. Bernard, M.S. Donley, Prog. Org. Coat. 41 (2001) 217.
[24] M.L. Zheludkewich, R. Serra, G. Grundmeier, L.H. Yang, M.G.S. Ferreira, Surf. Coat. Technol. 200 (2004) 4040.
[25] A. Conde, A. Durán, J.J. de Damborenea, Prog. Org. Coat. 46 (2003) 288.
[26] W.J.V. Ooij, D. Zhu, V. Palanivel, J.A. Lamar, M. Stacy, Silicon Chem. 3 (2006) 11.
[27] L.Y.L. Wu, E. Chwa, Z. Chen, X.T. Zeng, Thin Solid Films 516 (2008) 1056.
[28] F. Mammeri, E. Le Bourhis, L. Rozesa, C. Sanchez, J. Mater. Chem. 15 (2005) 3787.
[29] S. Pellice, P. Galliano, Y. Castro, A. Durán, J. Sol–Gel. Sci. Technol. 28 (2003) 81.
[30] S. Pellice, U. Gilabert, C. Solier, Y. Castro, A. Durán, J. Non-Cryst. Solids 348 (2004) 172.
[31] T. Linnert, P. Mulvaney, A. Henglein, H. Weller, J. Am. Chem. Soc. 112 (1990) 4657.
[32] Z. Zhang, R.C. Patel, R. Kothari, C.P. Johnson, S.E. Friberg, P.A. Aikens, J. Phys. Chem. B. 104 (2000) 1176.
[33] D.R. Brown, L. Kevan, J. Phys. Chem. 90 (1986) 1129.
[34] V.S. Gurin, N.E. Bogdanchikova, V.P. Pertanovskii, J. Phys. Chem. B 104 (2000) 12105.
[35] E.M. Egorova, A.A. Revina, Colloids Surf. A 168 (2000) 87.
[36] L.M. Liz-Marzán, I. Lado-Touriño, Langmuir 12 (1996) 3585.
[37] M. Epifani, C. Giannini, L. Tapfer, L. Vasanelli, J. Am. Ceram. Soc. 83 (2000) 2385.
[38] N.C. Rosero-Navarro, S.A. Pellice, Y. Castro, M. Aparicio, A. Durán, Surf. Coat. Technol. 203 (2009) 1897.
[39] A. Henglein, P. Mulvaney, T. Linnert, Electrochim. Acta 36 (1991) 1743.